Scanning Electron Microscopy and the Growth and Mechanical Properties of Cu_2O Scales

I. A. Menzies and P. Aldred

Corrosion Laboratories, Department of Chemical Engineering,
University of Manchester Institute of Science and Technology, Manchester, England

ABSTRACT

The morphology of growth of Cu_2O on Cu has been studied using scanning electron microscopy. The mechanical properties of columnar Cu_2O specimens prepared by total oxidation of metallic copper have been studied as a function of bend rate and temperature. The modulus of elasticity of cuprous oxide was constant ($\sim 4 \times 10^6$ psi) from room temperature to 500°C and thereafter decreased linearly with increasing temperature to $\sim 2 \times 10^6$ psi at 800°C. The oxide exhibited a pseudo brittle-ductile transformation at 360°C and 400°-500°C when slow and fast bending rates, respectively, were used. There was also a maximum strength peak at a critical temperature related to the onset of plastic deformation. Load-deflection functions indicated large amounts of plastic deformation and in the light of fracture surface observations this can be interpreted in terms of a slow cleavage mechanism.

Although a knowledge of the mechanical properties of oxide scales is important with respect to understanding completely the mechanisms of environmental degradation and breakdown of metals and alloys, few measurements of the mechanical properties of scales formed by thermal oxidation of the metal have been made. Tylecote (1) first attempted to measure the properties of copper oxide films on copper by a hot torsion method and more recently Harrison (2) has measured the fracture strain of Fe_3O_4 films formed on steel at 316°C in 2.5M NaOH at ambient temperature by an electrochemical method. Douglass (3) also presented evidence for the plasticity of ZrO_2 films on Zr at 500°C. None of the experimental techniques were completely satisfactory and most of the available information concerning properties has been obtained for oxide specimens produced by complete oxidation of the metal. The strength (4, 5) and creep (6) of iron oxides, the strength, elasticity, and creep of NiO (4, 7, 8) and the strength of Cu_2O (1) have all been measured. In the earlier investigations little attention was given to the effects of scale structure on properties and more recent studies of NiO (8, 9) indicated that the temperature of oxide growth and hydrogen annealing of nickel prior to oxidation had a significant effect on oxide structure and hence on properties. Strafford and Gartside (10) succeeded in establishing that the mechanical behavior of CoO is markedly affected by oxide stoichiometry and in particular that plastic deformation decreased as stoichiometry was approached and the number of cation vacancies decreased.

The present study of Cu_2O has been carried out to provide detailed structural and mechanical information for totally oxidized material to provide a suitable background for future studies of the properties of films attached to the metal. Oxide growth and fracture morphology have been investigated using scanning electron microscopy and the modulus of elasticity and the yield and fracture stress and strain studied as a function of loading rate and temperature. It was of particular interest to examine the onset and mechanism of plasticity in Cu_2O. It is anticipated that in the long term, this knowledge, with additional information concerning the properties of cupric oxide will permit a better understanding of certain aspects of the oxidation of copper to be achieved.

Experimental

Copper of 99.999% purity, in the form of 0.006 in. thick sheet by Metals Research Ltd., Cambridge, was used. No metallic impurities were detected by spectrographic methods. Standard specimens 0.3 cm broad and 3 cm long were oxidized in purified air at 1030°C for the required period of time to effect partial or complete oxidation of copper to Cu_2O.

The mechanical properties of the oxide specimens were measured using a three point loading bend technique (7, 9, 11). The apparatus used in the present work (11) was fully automatic and capable of measuring the properties up to 1200°C and under controlled atmosphere conditions. The load applied to the specimen and its central deflection were measured by a load cell and displacement transducer, respectively. The electrical outputs from the load cell and displacement transducer were fed into an X-Y autoplotter from which a load-deflection function was obtained. Bending rates of 0.011 and 0.508 cm/min were used throughout the work. The load-deflection functions were carefully analyzed to determine the modulus of elasticity, yield stress and strain, or fracture stress and strain as appropriate.

The modulus of elasticity (E) was calculated from the relationship $E = PL^3/4bd^3h$ where P is the load, L is the coupon length between its supports, b and d are the specimen width and thickness, respectively, and h is the measured deflection. Individually measured values of d must be used in order to maintain accuracy of the value of E. The fracture stress (Su) of specimens exhibiting only elastic deformation is given by $Su = 3PuL/2bd^2$ where Pu is the fracture load and the other terms have the same significance as above. The fracture strain (ϵ) of coupons exhibiting only elastic deformation is given by Su/E. If however the oxide coupons exhibit elastic and plastic deformation the methods outlined above for the calculation of stress and strain cannot be used. It can, however, be shown (11) that under these conditions the fracture strain is given by $\epsilon = 8hy/L^2\,red$ where y is $d/2$ and $L\,red \approx \sqrt{8hR}$ where R is the radius of curvature of the bent specimen. Furthermore it can be shown (12) that the stress (S) of a plastically bent rectangular section is given by

$$S = \frac{2}{bd^2}\,(2M + \phi\, dM/d\phi)$$

where M is the bending moment of the coupon and ϕ is half the angle subtended by two plane sections after bending. This relationship can be used to obtain the fracture stress when the coupons exhibit both elastic and plastic behavior (11).

Specimens for scanning electron microscopy were fractured either in the bend test apparatus or by hand while immersed in liquid nitrogen. The fractured samples of oxide or composite coupons were cemented to small Duralumin stubs by means of Durofix cement. The fracture surface was mounted normally to the stub and set at ~ 45° to the stub surface. In order to prevent surface charging of the specimen in the microscope the Durofix cement was coated with a thin layer of carbon black. A conducting path from the oxide sample to the Duralumin stub was also obtained using carbon black, great care being taken to avoid contamination of the fractured surface. The specimens thus prepared were examined in a Cambridge Instrument Company, Stereoscan Mk IIa. The theory of the instrument has been discussed by Oatley *et al.* (13) and will not be discussed here. The specimen detail resolution was always better than 500Å and as good as 150Å in some cases with a depth of focus at least 300 times greater than that of a normal light microscope.

Results

Morphology of oxide formation on copper.—An SCEM study was made of the nature of growth of Cu_2O. The structure of the Cu_2O film formed after 2 min at 1030°C is shown in Fig. 1a. It can be seen that a portion of the Cu_2O film has lifted straight off the Cu substrate during the fracture process. The Cu_2O film is compact and the metal-oxide interface is relatively smooth. After oxidation for 10 min at 1030°C the oxide was again compact although in one special area numerous voids were present (Fig. 1b). The pronounced markings in the Cu_2O film are cleavage steps produced by the fracture process and the points marked x in Fig. 1b are cleavage facets. The structure of a completely oxidized coupon is shown in Fig. 1c and a number of voids can be seen at the core of the coupon.

The structure of the oxide film formed at the corners of copper coupons was unusual and consisted of an outer columnar-grained layer and an inner fine-grained layer which exhibited numerous pores. The formation of this structure is shown clearly in the scanning electron micrographs in Fig. 2. The Cu-Cu_2O interface after only 2 min oxidation at 1030°C is shown in Fig. 2a. It is immediately apparent that Cu_2O crystallites (B) have grown at the interface beneath a compact columnar layer of Cu_2O and pores are associated with the crystallites. This area was found to have developed into a fine-grained porous structure after oxidation for 10 min at 1030°C (Fig. 2b). The remaining metal core is indicated in Fig. 2b and the finger-like crystallites of Cu_2O, observed in Fig. 2a, can be seen growing from this region near the corner of the Cu-Cu_2O interface. An extremely porous and confused mass of small crystals is shown in Fig. 2c. Detailed examinations of specimens after total oxidation indicated the presence of large holes and small grains of Cu_2O in the specimen center between the outer compact columnar-grained layers of Cu_2O (*cf.* Fig. 1c). It was now of interest to measure the mechanical properties of such totally oxidized coupons and to examine the fracture surfaces in some detail.

Effect of measurement temperature, atmosphere, and bending rate on the mechanical behavior of Cu_2O *coupons.*—The properties of the coupons were measured at temperatures ranging from ambient to 800°C in both Ar and O_2 atmospheres. Over-all the load-deflection functions and mechanical properties were found to be the same for both Ar and O_2 atmospheres. For the slow bending rate, the Cu_2O coupons exhibited elastic behavior prior to fracture at 325°C whereas at 360°C some plastic deformation was also observed (Fig. 3). The amount of plastic deformation observed at 360°C was such that some coupons were unbroken at the maximum deformation limit of the apparatus and hence the properties were not investigated at higher temperatures. For the fast bending rate elastic behavior to fracture was observed at 325°, 360°, and 400°C and plastic deformation was only observed

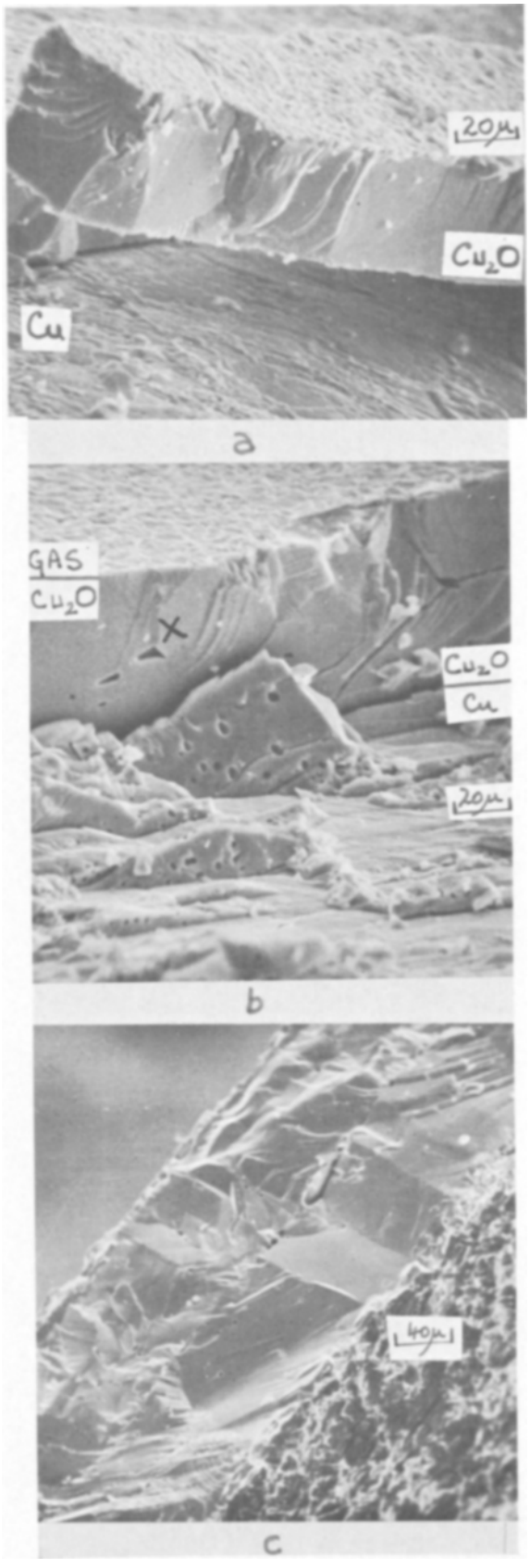

Fig. 1. Fracture surfaces of Cu or Cu_2O specimens. (a) Cu specimen after partial oxidation for 2 min in air at 1030°C. (b) Cu specimen after partial oxidation for 10 min in air at 1030°C; isolated area near edge showing marked porosity in Cu_2O film. (c) Cu_2O specimen produced by total oxidation of Cu in air at 1030°C after bending at the slow rate at 360°C in argon.

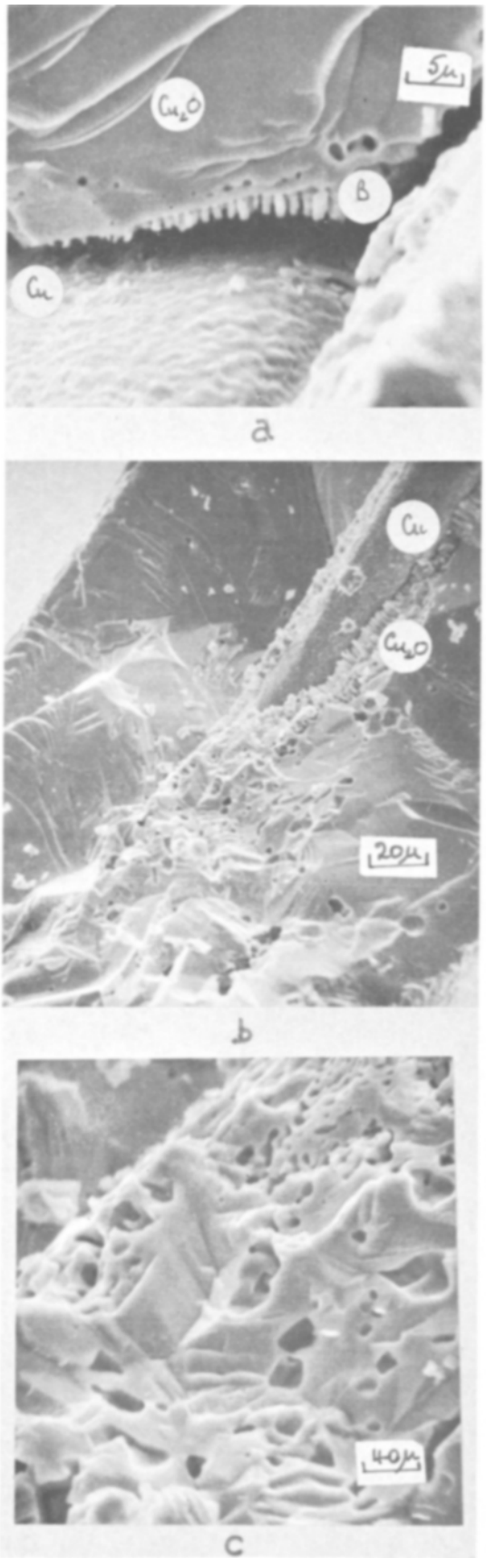

Fig. 2. Details of Cu-Cu_2O interface and of porosity in Cu_2O films. (a) Metal-oxide interface at specimen corner after 2 min oxidation in air at 1030°C. (b) General view of metal-oxide interface; exposure as in (a). (c) Details of porous region in specimen (b).

at temperatures > 500°C. The load-deflection functions obtained at both bending rates exhibited marked

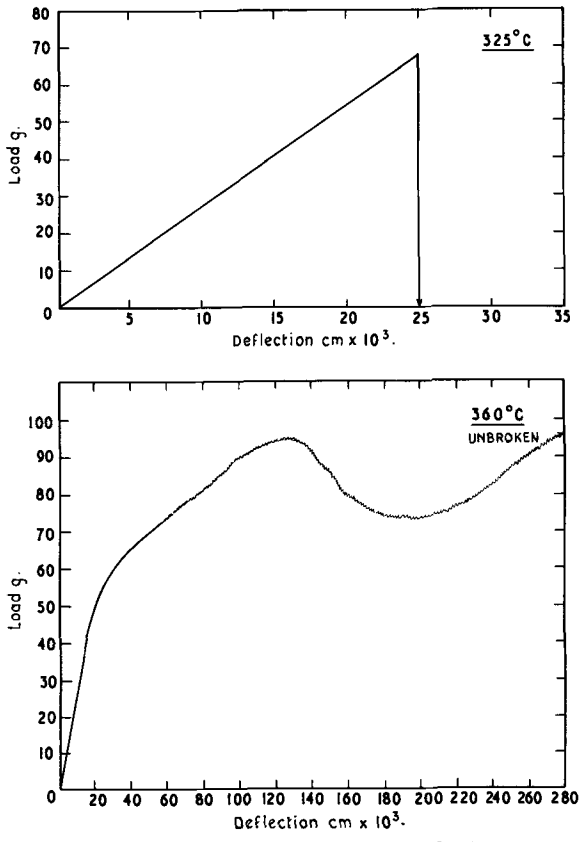

Fig. 3. Load-deflection functions obtained for Cu_2O specimens at the slow bending rate (0.011 cm/min) in O_2 or argon at 325° and 360°C.

serrations when the Cu_2O coupons were plastically deformed to an amount > 65 x 10^{-3} cm (Fig. 3).

The mechanical properties of the Cu_2O coupons were calculated from the load-deflection functions and the results are given as a function of temperature in Tables I and II for the slow and fast bending rates, respectively. The modulus of elasticity was independent of the bending rate and was constant at ~4 × 10^6 psi when the temperature was increased from ambient

Table I. Mechanical properties of Cu_2O coupons bent at 0.011 cm/min as a function of temperature

Temperature, °C	Oxide yield strain, %	Oxide fracture strain, %	Oxide modulus of elasticity, psi × 10^{-6}	Oxide yield stress, tsi	Oxide fracture stress, tsi
Ambient	—	0.15 (0.01)	4.0 (0.5)	—	2.7 (0.5)
325	—	0.22 (0.01)	3.8 (0.5)	—	3.7 (0.5)
360	0.11 (0.02)	0.56/7.8	4.2 (0.5)	2.1 (0.3)	—

Standard deviation values are given in parentheses.

Table II. Mechanical properties of Cu_2O coupons bent at 0.508 cm/min as a function of temperature

Temperature, °C	Oxide yield strain, %	Oxide fracture strain, %	Oxide modulus of elasticity, psi × 10^{-6}	Oxide yield stress, tsi	Oxide fracture stress, tsi
Ambient	—	0.17 (0.01)	4.0 (0.5)	—	3.1 (0.5)
325	—	0.19 (0.01)	4.0 (0.5)	—	3.4 (0.5)
360	—	0.23 (0.02)	4.2 (0.5)	—	4.2 (0.5)
400	—	0.23 (0.02)	4.2 (0.4)	—	4.2 (0.5)
500	0.065 (0.005)	—	4.2 (0.5)	1.2 (0.2)	—
600	0.032 (0.003)	—	3.5 (0.5)	0.5 (0.1)	—
700	0.027 (0.002)	—	2.5 (0.5)	0.3 (0.05)	—
800	0.014 (0.002)	—	2.0 (0.3)	0.1 (0.02)	—

Standard deviation values are given in parentheses.

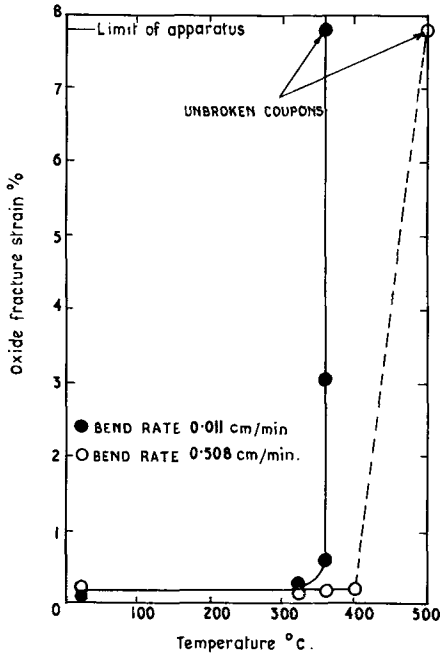

Fig. 4. Fracture strain of Cu_2O coupons as a function of the measurement temperature and bending rate.

to 500°C. Above 500°C a rapid decrease in the modulus of elasticity from $\sim 4 \times 10^6$ psi to 2×10^6 psi was observed when the temperature was increased to 800°C. The Cu_2O coupon fracture strain is shown as a function of the bending rate and temperature in Fig. 4 in order to bring out clearly the presence of a pseudo brittle-ductile transformation which was dependent on the bending rate. For the slow bending rate the transformation occurred at ~360°C, whereas for the fast bending rate the transformation was delayed to some temperature between 400° and 500°C. At temperatures above the transformation temperature Cu_2O specimens remained unbroken after 7.8% strain (apparatus limit) for both bending rates. The fracture strain of the oxide specimens at temperatures below the transformation temperature increased from 0.16 to 0.23% when the temperature was increased from ambient to just below the transformation temperature for each bending rate. In this temperature range the fracture stress remained constant at ~3-4 tsi. Finally, it is clear that the yield strain and yield stress of the Cu_2O coupons bent at the fast rate decreased from 0.065 to 0.014% and from 1.2 to 0.1 tsi, respectively, when the temperature was increased from 500° to 800°C.

Microscopic examination of mechanically deformed Cu_2O *specimens.*—A Cu_2O specimen after bending at 360°C in an argon atmosphere is shown in Fig. 5. Examination of the surface topography of such specimens indicated by the presence of numerous slip lines and few deformation bands that plastic deformation had occurred during bending. Other specimens bent to fracture at the slow rate were examined with the SCEM. A typical area of the fracture surface is shown in Fig. 6a and in more detail in Fig. 6b. A comparison of these figures shows that the nature of the crack front, commencing at point x (Fig. 6a) was complex. A separate area of the fracture surface is shown in Fig. 6c, and this provides evidence that fracture occurred at 360°C both by transgranular and intergranular crack propagation. The crack front propagated in the direction shown by the arrows. Originally the crack progressed in a transgranular manner then in the vicinity of the arrows it changed partially to an intergranular front (indicated by the solid arrows) while the remainder continued in a transgranular manner across another grain (dotted arrows).

Discussion

The SCEM study of the growth of Cu_2O on copper confirms the columnar nature of the grains and the smooth nature of the oxide-metal interface in general (Fig. 1a). The formation of isolated crystallites and oxide bridges at the corners of specimens (Fig. 2a, b) was of especial interest. This has most probably arisen due to the severe mechanical constraint at the corners which has prevented plastic flow of the oxide.

It is also clear from the present work that there was no significant difference in the properties of Cu_2O as a function of atmosphere (Tables I and II). Thus under these conditions the same results were obtained whether the measurements were made in argon or oxygen at atmospheric pressure. There was thus no indication of changes in properties of the specimens with possible changes in vacancy distribution across the scales.

There are few absolute values of elastic modulus for Cu_2O in the literature. Dankov and Churaev (14), however, suggested that a value $\sim 3 \times 10^6$ psi was typical for Cu_2O at ambient temperature. They obtained this value indirectly from internal stress measurements and the agreement with the measured value of 4×10^6 psi in the present work is satisfactory. The rapid decrease in the modulus of elasticity at a critical temperature is a common occurrence in metals and oxides, *e.g.*, in polycrystalline MgO at ~ 1000°C (15, 16), and it has been suggested (17) that this rapid decrease may be caused by grain boundary sliding. Since this can be an important deformation mechanism at temperatures > 0.5 Tm (Tm for Cu_2O ~ 460°C) the decrease in modulus of elasticity at 500°C would be in reasonable agreement with a grain boundary sliding mechanism. This will be discussed more fully later with respect to fracture.

The yield strain and stress of Cu_2O specimens decreased with increasing temperature from 500° to 800° (Table II). This is in agreement with the fact that an increase in temperature increases dislocation mobility thus facilitating plastic flow at lower stresses. The values obtained are in excellent agreement with those obtained (18) from compression experiments at similar temperatures at a crosshead speed of 0.13 cm/min, *i.e.*, between the two values used in the present work. However, Vagnard and Washburn found that yielding occurred at 200°C and not at 400°-500°C as observed for the fast bending rate in the present work. Compressional experiments are better suited for observing plastic deformation in oxide materials because the tensile stresses which develop in bending accentuate brittleness and therefore higher temperatures will be required to initiate yielding in bending.

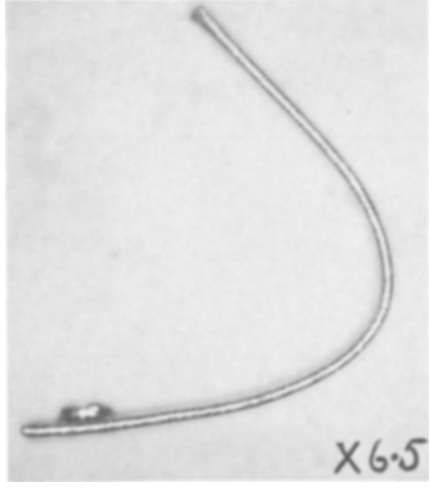

Fig. 5. Cu_2O specimen after bending at the slow rate (0.011 cm/min) at 360°C. X6.5.

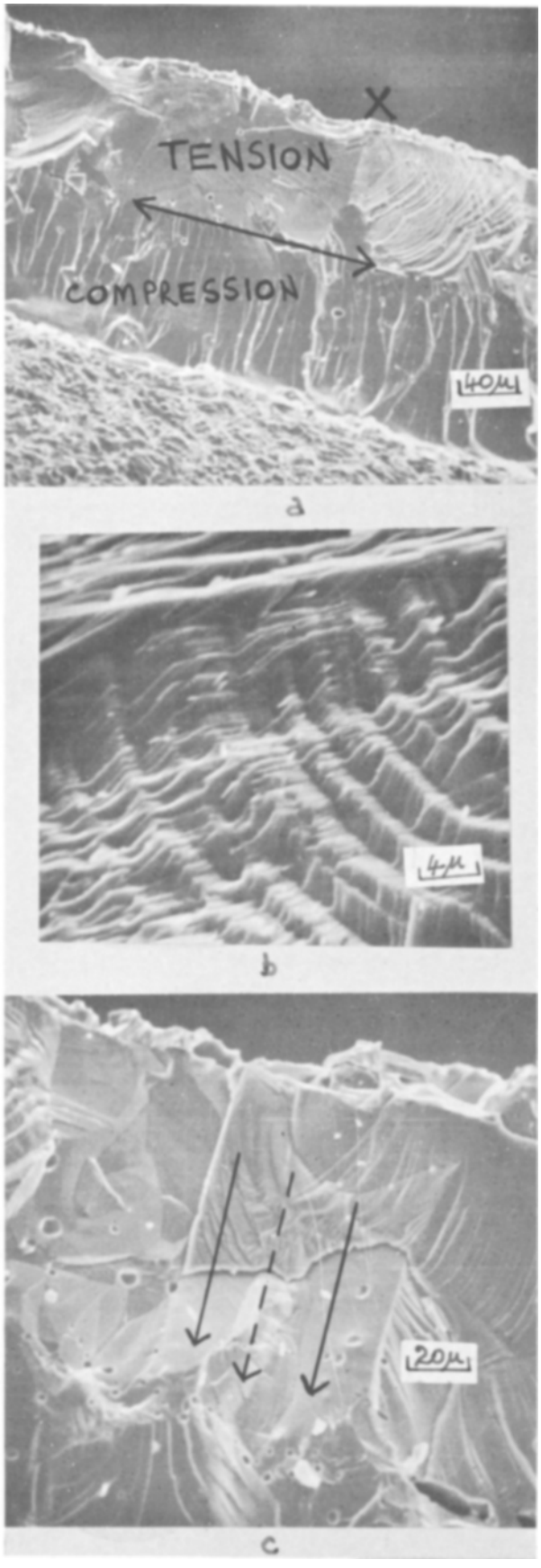

Fig. 6. Fracture surfaces of Cu_2O coupon after 3.6% strain at 360°C in argon at the slow bend rate (0.011 cm/min). (a) General view. (b) Detail of cleavage facets on tensile side of neutral axis. (c) Additional aspects of tensile side of neutral axis.

The fracture strains of Cu_2O at temperatures below the pseudo brittle-ductile transformation temperature are in agreement with the fracture strains observed in brittle materials (19). At temperatures greater than the transition temperature the observed strains of $\geq$7.8% before fracture can be compared with previous work (1) in which Cu_2O elongations of ~12% and ~25% were observed at 500°-600°C and 700°-900°C, respectively. The observation that plastic deformation is observed at lower temperatures (~360°C) with a slow bend rate is in general agreement with observations in metals where the flow stress is increased by an increased strain rate (20). Over-all the yield stress corresponding to the onset of plastic deformation was lower at higher temperatures (*cf.* Table II), in further agreement with the mechanical behavior of metals. Since the flow stress is the stress required to initiate plastic deformation it will depend on such material factors as purity, grain size, and crystal structure. In the case of Cu_2O here this is of high purity and of large columnar grain structure. The relatively easy deformation of Cu_2O is reflected in the relatively low yield stress at all temperatures and the relatively high fracture strains. Cuprous oxide has an unusual structure (18) in that oxygen atoms are ordered on a b.c.c. lattice and the copper atoms occupy the sites of an f.c.c. lattice. The structure consists of two interpenetrating and identical networks which are not cross-connected by any primary Cu-O bonds. Slip lines have been observed on the tensile surfaces of Cu_2O but examination of specimens after fracture at 360°C (Fig. 6a) did not show any dimple formations which are characteristic of ductile fractures (21). In contrast the fracture surfaces exhibited cleavage with some isolated areas showing intergranular fracture. These observations are in contrast to the shape of the load-deflection functions (Fig. 3) which suggest extensive plastic deformation. Observations on the Cu_2O specimens strongly suggest that slow cleavage is responsible for the shape of the load-deflection functions of the type shown in Fig. 3. Surface cracks were also found in the Cu_2O specimens. This was also observed in Cu_2O by Vagnard and Washburn (18) during compressional experiments at <400°C. They found that cracks nucleated at local stress concentrations where slip bands crossed and also where they met grain boundaries. A similar type of crack nucleation has been observed in MgO (22, 23) and analyzed by Stroh (24, 25). It seems likely that cracks observed in the present work nucleated in the manner described by Vagnard and Washburn, since large local deformations were observed at slip band intersections (Fig. 7a) and also where slip lines piled up at a grain boundary (Fig. 7b). This inhomogeneity of slip observed in this system could offer a possible explanation for the complicated shape of the load-deflection function in Fig. 3. The peaks in the plastic region of the curve were observed continuously up to deformations of ~800 x 10^{-3} cm and it seems possible that these peaks are associated with the initiation of slip in grains which, up to that point, were undeformed. The increase in work hardening observed after the initial yield point will be due to grain boundary and crystallographic blockages which oppose slip. At some critical strain these blockages will be overcome and slip will be initiated in neighboring grains. When this occurs there will be an initial decrease in the work hardening rate followed by an increase as further slip becomes blocked. This process will repeat itself giving rise to the observed peaks in the load-deflection functions.

Once surface cracks have formed their rate of propagation will depend on the bending rate, temperature, and degree of plastic relaxation at the crack tip. This plastic relaxation absorbs energy and prevents rapid crack propagation (26). In fact it has been observed that cracks have propagated through Cu_2O grains which do not exhibit slip deformation and that crack propagation has been halted at the grain exhibiting extensive slip deformation. The cracks prop-

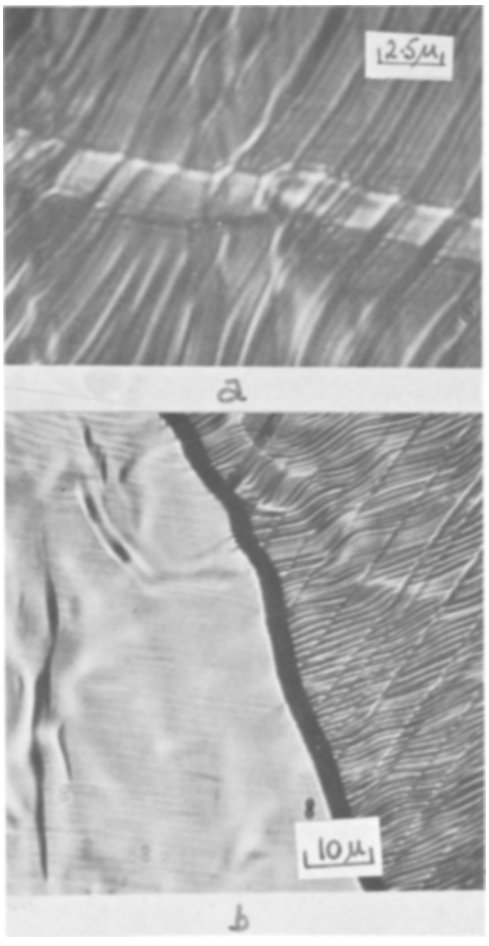

Fig. 7. Surface topography of Cu_2O specimen, formed in air at 1030°C, after bending at 360°C in argon. (a) Intersection of slip bands. (b) Intersection of slip lines with a grain boundary.

agate by repeated breaking of crystal bonds at the crack tip. In Cu_2O the {111} planes have weak bonds and cleavage occurs along them (18). During bending therefore, slow cleavage on {111} planes would be expected if most of the surface energy, created by crack formation, was absorbed by plastic deformation. Such plastic deformation during cleavage of ionic crystals has been observed even at ambient temperatures (27) and hence at the higher temperatures in the present work plastic relaxation is even more favored. The fracture surface of a Cu_2O specimen (Fig. 6a) indicates that a crack was initiated at a grain boundary marked x on the tensile side of the neutral axis. To the left of the boundary, cleavage occurred mainly on one crystal plane within the large grain, whereas to the right of the boundary a complicated crack front was observed (Fig. 6b). It would appear that this crack front could be described by two main vectors situated at 90° to each other. At the same time as the crack front was moving directly perpendicular to the neutral axis it was also moving parallel with this axis. The resultant crack front was therefore most likely situated at ~45° to the point marked x in Fig. 6a. It can be visualized that this duplex direction of crack propagation would produce a "tearing" effect resulting in a confused structure (cf. Fig. 6b). It can be seen in Fig. 6b that numerous small cleavage steps are associated with larger cleavage steps which are situated at ~90° to each other and could therefore represent cleavage on the {111} planes. It is suggested therefore that during bending cracks are nucleated on the tensile surface. These cracks are prevented from drastic propagation by plastic relaxation at the crack tip. Bending continues and the stress at the crack tip builds up until it is sufficient to cause further propagation of the crack which in turn is halted by plastic relaxation. This process will be continuous and the crack propagates slowly along the {111} planes. This intermittent crack propagation is probably responsible for the serrations in the load-deflection function. Gilman *et al.* (28) have shown that the increases in surface energy that accompany cleavage step formation in ionic crystals may cause the cracks to move more slowly than they would normally do under the same driving force. Thus the suggested crack propagation mechanism would account for the shape of the load-deflection functions and the lack of evidence in the oxide fracture surfaces for extensive ductility.

Finally the strength peak observed at a temperature immediately below that for which plastic deformation was observed (Tables I and II) requires comment. A similar phenomenon has been reported previously for Cu_2O wires (1) and for NiO wires and sheet specimens (4, 8). Silicon and germanium also exhibit such strength peaks with increasing temperatures (29). The strength will tend to rise as the heat-induced ability to deform plastically increases with temperature. Plastic deformation relieves stress concentrations and thereby promotes the full strength properties of the material. Above the temperature of maximum strength, the strength decreases with further increase in temperature, as in the case of ductile metals.

Acknowledgments

We wish to thank Professor T. K. Ross for the provision of research facilities and one of us (P.A.) wishes to thank the Science Research Council for the award of a research studentship. We also wish to thank Mrs. P. Cross of the Department of Textile Technology for her valued advice and assistance with the SCEM study.

Manuscript submitted Jan. 24, 1969; revised manuscript received June 12, 1969.

Any discussion of this paper will appear in a Discussion Section to be published in the June 1970 JOURNAL.

REFERENCES

1. R. F. Tylecote, *J. Inst. Metals*, **78**, 301 (1950).
2. P. L. Harrison, *Corrosion Sci.*, **7**, 789 (1967).
3. D. L. Douglass, *ibid.*, **5**, 255 (1965).
4. R. F. Tylecote, *J. Iron Steel Inst.*, **196**, 135 (1960).
5. J. Vagnard and J. Manenc, *Mem. Sci. Rev. Met.*, **62**, 251 (1965).
6. J. D. Mackenzie and C. E. Birchenall, *Corrosion*, **13**, 783 (1957).
7. I. A. Menzies and K. N. Strafford, *J. Mater. Sci.*, **2**, 358 (1967).
8. P. Aldred, M. Sc. Thesis, Manchester, England 1966.
9. I. A. Menzies and P. Aldred, *Corrosion Sci.*, **8**, 525 (1968).
10. K. N. Strafford and H. Gartside, *Nature*, **220**, 158 (1968).
11. I. A. Menzies and P. Aldred, In press.
12. A. Nadai, "Theory of Flow and Fracture in Solids," Vol. 1, p. 359, McGraw Hill, London (1950).
13. C. W. Oatley, W. C. Nixon, and R. F. W. Pease, "Advances in Electronics and Electron Physics," Vol. 21, p. 181, Academic Press, New York (1965).
14. P. D. Dankov and P. V. Churaev, *Dokl. Akad. Nauk. SSSR.*, **73**, 1221 (1950).
15. B. Schwartz, *J. Am. Ceram. Soc.*, **35** (12), 325 (1952).
16. R. M. Spriggs, T. Vasilos, and J. B. Mitchell, *ibid.*, **47** (12), 606 (1964).
17. R. L. Coble and W. D. Kingery, *ibid.*, **39** (11), 377 (1956).
18. G. Vagnard and J. Washburn, *ibid.*, **51** (2), 88 (1968).
19. N. F. Astbury, Brit. Ceram. Res. Assn., Research paper No. 504 (1961).
20. A. G. Guy, "Elements of Physical Metallurgy," 2nd Ed., Addison-Wesley Publishing Co. (1960).
21. R. M. N. Pillaux, *Metals Eng. Quart.*, **5** (4), 26 (1965).
22. R. J. Stokes, T. L. Johnston, and C. H. Li, *Phil. Mag.*, **4**, 920 (1959).

23. W. G. Johnston, *ibid.*, **5**, 407 (1960).
24. A. N. Stroh, *Proc. Roy. Soc.* (*Lond*), **A 223**, 404, (1954); **232**, 548 (1955).
25. A. N. Stroh, *Advances in Phys.*, **6**, 418 (1957).
26. A. R. C. Westwood and M. H. Kamdar, *Phil. Mag.*, **8**, 878 (1963).
27. C. T. Forwood and B. R. Lawn, *ibid.*, **13**, 595 (1966).
28. J. J. Gilman, C. Knudsen, and W. Walsh, *J. App. Phys.*, **29**, 601 (1958).
29. E. M. Savitsky, "The Influence of Temperature on the Mechanical Properties of Metals and Alloys," Oxford Univ. Press, London (1962).

The Free Energy of Formation of Tantalum Silicides Using Solid Oxide Electrolytes

S. R. Levine and M. Kolodney*

The City College of The City University of New York, New York, New York

ABSTRACT

A method is described for determining the standard free energies of formation of the tantalum silicides from emf measurements on cells with solid thoria-yttria electrolytes. Measurements were conducted over the temperature range 900°-1100°C in a purified argon atmosphere. Corrections for electronic conduction were established with Ta, Ta_2O_5 electrodes. Difficulties were encountered because the hard, refractory nature of the compounds prevented fabrication of dense electrodes and because silica films interfered with the measurements. At 1300°K, the measured standard free energies of formation in kcal per gram atom of silicon are: $TaSi_2$, —8.1 (+1.8/—3.7); Ta_5Si_3, —24.0 ±3; Ta_2Si, —27.2 ±3.1; $Ta_{4.5}Si$, —37.3 ±7.2.

Silicides are of interest as protective coatings for tantalum and other refractory metal alloys exposed to oxidizing conditions. Since the formation of a silica glass is essential for protection, a desirable reaction is one that produces silica and a lower silicide, as for example

$$5TaSi_2 + 7\,O_2 = 7SiO_2 + Ta_5Si_3 \qquad [1]$$

On the other hand, since the formation of the oxide of the substrate may interfere with the integrity of the silica film, the following reaction is undesirable

$$4TaSi_2 + 13\,O_2 = 2Ta_2O_5 + 8SiO_2 \qquad [2]$$

However, the refractory metal oxide may be tolerable where SiO_2 and the metal oxide form a glass or where the metallic oxide is volatile (1, 2).

In order to predict and understand the oxidation behavior of refractory metal silicides accurate free energy of formation data are required for the silicides and their oxidation products. Data for silica and for the refractory metal oxides are available (3), but data for silicides are scanty. Free energies of formation are known only for some of the rhenium silicides (4). For most other refractory metal silicides only enthalpies of formation are available. Thermodynamic information on the tantalum-silicon system, which is the subject of this study, has been collected by three classical techniques: Brewer and Krikorian (5) determined limits for the stability of refractory silicides by direct reaction of the compounds with carbides and nitrides. Robins and Jenkins (6) measured the heats of formation of some transition metal silicides from the heat evolved during formation of the compounds from their elements. In the third technique, employed by Searcy and co-workers (7-9), the dissociation pressure of silicon over the silicide of interest was measured by the Knudsen effusion method. The vapor pressure data were analyzed by a Second or Third Law approach to obtain enthalpies of formation for the silicides. Data for the tantalum silicides, obtained by these three techniques are presented in Table I. The values listed in column IV are based on an average of the Second and Third Law techniques using a value of —112 kcal for the heat of sublimation of silicon at 298°K. The values in column V are based on the same vapor pressure data as column IV but an improved value of the heat of sublimation of silicon (—108.4 kcal at 298°K) was used and the calculations were made using only the Third Law method (10, 11).

In the present work a fourth method was for the first time applied to the determination of the thermodynamic properties of the tantalum silicides. This technique employs a solid oxide electrolyte between a silicide electrode and a reference electrode. Solid electrolytes for the measurement of thermodynamic properties were brought into prominence by Kiukkola and Wagner (12), Schmalzried (13), and others. Oxide electrolytes are binary oxides which conduct almost entirely by transport of oxygen ions over a given temperature-oxygen partial pressure domain. A simple cell employing an oxide electrolyte and an iron-iron oxide (Fe_xO) reference electrode may be formulated as

$$Pt/Fe,Fe_xO//\text{oxide electrolyte}//M,MO/Pt \qquad [3]$$

where the cell reaction is

$$M + Fe_xO = MO + xFe \qquad [4]$$

If the cell is reversible, the free energy of the reaction

Table I. Enthalpy of formation data for the tantalum silicides (kcal/g-atom of silicon)

I Compound	II Brewer and Krikorian (5), $\Delta H°_{298}$	III Robins and Jenkins (6), $\Delta H°_T$	IV Myers and Searcy (7), $\Delta H°_{298}$	V Searcy and Finney (10), $\Delta H°_{298}$
1/2 $TaSi_2$	−12.8 to −32.3	−13.9 ± 1	−11.6 ± 5	−12 ± 3
1/3 Ta_5Si_3	−20 to −77.2	−25.3 ± 1	−26.7 ± 5	−24 ± 4
Ta_2Si	−20 to −90.1	—	−29.3 ± 5	−30.2 ± 4
$Ta_{4.5}Si$	−20	—	−34.4 ± 5	−35.8 ± 4

* Electrochemical Society Active Member.

Keywords: silicides, tantalum silicides, solid electrolytes, free energies of formation, emf measurements, electronic conduction.